This paper appears in IEEE Transactions on Control Systems Technology, 2019
DOI: 10.1109/TCST.2019.2944117

Image-Guided Observer-Based Control for Needle Steering

Bita Fallahi[1], Ronald Sloboda [2], Nawaid Usmani [2], and Mahdi Tavakoli [1]

***Abstract*—In robot-assisted needle insertion procedures, in order to steer a beveled-tip needle toward a target location, the needle tip pose is required to be used as feedback. Mathematically, the needle tip pose can be expressed as a position vector and a rotation matrix that represents the orientation of the needle. Using the traditional two dimensional (2D) ultrasound imaging modality, since the images are low in resolution and the needles are small in diameter, only the position of the needle tip can be measured, and the orientation information cannot be directly extracted. This paper presents a nonlinear observer for estimating the needle tip orientation based on needle three dimensional (3D) kinematic equations and the position data measured from ultrasound images. Assuming bounded inputs for the needle model, it is shown that the observation error remains bounded. The performance of the observer is shown in an observer/controller feedback loop. The stability and convergence of the observer/controller combination are shown by solving Linear Matrix Inequality (LMI) optimizations. Experiments performed for different tissue types and different needle insertion goals verify the effectiveness of our method.**

***Keywords*—Needle Steering; Observer; State Feedback Control**

I. Introduction

Needle insertion procedures are used in many minimally invasive surgeries to access a target organ for diagnosis, sample removal or drug delivery. In these procedures, the needle tip positioning accuracy is a crucial factor in determining surgical outcomes. Using beveled-tip needles, due to the asymmetric interaction forces acting at the tip, the needles bend during the insertion. Manipulating the needle base outside the body provides a means to change the needle path and to steer it towards the desired location inside the tissue.

In robot-assisted needle insertion procedures, controllers are designed to produce necessary control actions using the needle's current states. Needle tracking inside the tissue can be performed using different measurement methods such as fiber Bragg grating sensors [1], different imaging modalities [2], [3], and electromagnetic tracking [4], [5]. In general, for clinical applications, it is preferred to use measurements performed from outside of the body as they impose least limitations on measurement equipment dimension and sterilization issues. In this regard, force measurements at the needle base and imaging modalities such as ultrasound and Computed Tomography (CT) are suitable methods which provide estimates of the needle shape and tip position. In [6], the needle base force data is combined with mathematical models to find the needle tip position. Obviously, having access to the needle states simplifies the controller design and improves the performance of the system.

During the insertion, the needle moves on a 3D curved path. There have been many different motion planners proposed for needle steering. In these methods, the needle tip information is combined with mathematical models and re-planning is performed to find the required action at the current moment and the future times to reach the desired position [7], [8]. In [9], a two-body rigid/flexible model for the needle is proposed and used for steering the needle in soft tissue. In other methods, the steering problem is based on a feedback control loop where the controller calculates the control action just for the current time for making the tip positioning error small [4], [10]–[12]. In [10] the needle's tip planar motion is controlled using only the information about the tip position as the feedback signal. In [4], the needle tip orientation is found using a five-degree-of-freedom (DOF) sensor and used in calculating the control signals.

B-mode ultrasound images with 1D transducers are very common and cost-effective methods for tracking instruments and tissue in clinical settings, using which the needle tip position can be extracted from 2D images [13]. However, ultrasound images can only provide the needle tip position in Cartesian space as due to the low-resolution ultrasound images and the small diameter of the needle, the bevel orientation cannot be detected in the images. In such cases, model-based observers can be designed to estimate the non-measurable system states. In [11], state transformations are used to form a set of linear equations for which a linear observer is developed and used with a linear controller to keep the needle in one plane. Later, this observer is used in many other works. Authors in [14] employed the linear observer to estimate the needle tip orientation and used the estimated variables in a low-level controller, which works along with a high level 2D planner to steer the needle on the optimal path. In [12], the same transformation is used, and a nonlinear observer is designed to be used with an adaptive controller. In [15] this linear observer is designed for the reduced configuration space and is fed to the fiber space observer to estimate the full system states for a planar task. In [16] a model for torsional dynamics of the needle is presented and augmented with planar variables. The system is then linearized and a Kalman filter is employed

This work was supported by the Natural Sciences and Engineering Research Council (NSERC) of Canada under grant CHRP 446520, the Canadian Institutes of Health Research (CIHR) under grant CPG 127768, and by the Alberta Innovates - Health Solutions (AIHS) under grant CRIO 201201232.

∗ Correspondence: Bita Fallahi, Department of Electrical and Computer Engineering, University of Alberta, 11-203 Donadeo Innovation Centre for Engineering, 9211-116 Street NW, Edmonton, AB, T6G 1H9, Canada. E-mail: fallahi@ualberta.ca

[1]B. Fallahi and M. Tavakoli, PhD, are with the Department of Electrical and Computer Engineering, University of Alberta, 11-203 Donadeo Innovation Centre for Engineering, 9211-116 Street NW, Edmonton, AB, T6G 1H9, Canada. E-mail: {fallahi, mahdi.tavakoli}@ualberta.ca

[2]R. Sloboda and N. Usmani are with the Cross Cancer Institute and the Department of Oncology, University of Alberta, Edmonton, Edmonton, Canada T6G 1Z2. E-mail: {ron.sloboda, nawaid.usmani}@albertahealthservices.ca.

to estimate the system states and apply a state feedback control. Usign Kalman filters, in [5], multiple sensor information is used along with a Kalman filter. Authors in [17] employed an unscented Kalman filter and 3D ultrasound images. In this work, one of the orientation angles is considered to be known as a measurement using a simplifying assumption. In [18], we designed a nonlinear observer to partially estimate the needle tip orientation. In this work, the stability and convergence of the observer were only guaranteed for a limited workspace.

In the current work, an approximate high-gain observer is used to estimate the rotation matrix representing the needle tip orientation. Considering an upper-bounded input signal for the needle model, the proposed observer is shown to be stable even at singularities, which guarantees the boundedness of the observation error. As we will see later, the needle model inputs comprise of needle insertion velocity and needle base rotational velocity. Moreover, the upper bound of the error can be obtained in terms of the observer gain, system parameters and the input upper bound.

II. Contributions

The needle steering problem involves finding algorithms for rotating the needle at its base during the insertion to reach the desired deflection. Due to the asymmetry of the forces at the beveled tip, rotating the needle and changing the bevel orientation affects the needle path inside the tissue. Since this path depends on the tip orientation, having access to the needle tip pose information, i.e., its Cartesian position and orientation will be helpful for accurate needle steering. The needle tip pose can be measured using different methods; however, these methods should satisfy the clinical requirements. Ultrasound imaging is a low-cost non-invasive imaging modality, which has been widely used in clinical applications. Image processing techniques can be applied on the ultrasound images to provide measurements of the needle tip position; however, since the ultrasound images fail to provide high-resolution images and the needles used in needle insertion procedures are also very small in diameter, the needle tip orientation cannot be measured using this imaging modality. Moreover, due to the sterilization issues, the use of needle-mounted sensors is not clinically feasible. Alternatively, using the measured variables, i.e., the position data and the mathematical models for the needle-tissue interaction, state observers provide a method to get an estimate of the needle tip orientation [11], [18], [19]. In this paper, the 3D unicycle equations [20] are used. It is shown that without any state transformations the needle kinematics can be written as three subsystems including linear terms. Although these equations are simple, they fail to meet the Lipschitz continuity condition, which makes the observer design more challenging. To overcome this limitation, the method introduced in [21] is used which deals with non-Lipschitz systems. This method uses 2D ultrasound images and compared with other observers mentioned in Section I, does not impose any limitation on the operation region as it deals with the singularities. However, this method can only guarantee the boundedness of the observation error, i.e., the difference between the actual and the estimated needle tip orientation. The observer gain can be selected properly to achieve the desired error bound. When combined with a closed-loop controller, this is sufficient for satisfactory needle tip positioning performance.

Remembering the main goal of designing an observer, the estimated states should be used in a properly designed controller to compensate for the positioning errors. The observer/controller combination, however, should be designed such that the stability and performance of both the controller and the observer are guaranteed. As with any observer, a requirement of the proposed observer is to have a bounded input signal for the system, or equivalently a bounded control input in a feedback configuration. This leads to the idea of limiting the control signal before applying to the system and designing the controller accordingly. This assumption is not very limiting as in practice eventually the actuators saturate, which can be considered as having an upper-bounded control signal. Nevertheless, saturation should be considered in the controller design to ensure the stability and performance of the observer-based controller.

The observation error and the introduced saturation on the control signal are considered as an additive uncertainty. Taking the uncertainty into account, a parametrized state feedback controller is designed using pole placement method and is analyzed using LMI optimizations to find the region of attraction for the tracking error.

In this paper, the stability of the whole system is guaranteed by stabilization of the observer and designing a stable controller such that the observer requirements are met. To this end, the paper is divided into two parts. The first part overviews the state observer for estimating the needle tip states and the second part is devoted to designing a controller, which acts along with the designed observer. The paper is organized as follow. Section III presents a review of the needle model. Section IV provides the observer structure and its proof of stability. In Section V the controller design and analysis procedure are presented, and in Section VI the proposed observer/controller structure is validated using experiments.

III. Nonholonomic Modeling of Needle Motion

During the insertion of beveled-tip needles, the asymmetric interaction forces acting at the needle tip cause the needle to bend toward the bevel orientation. Axially rotating the needle base changes the bevel orientation making the needle follow a 3D curved trajectory. The needle motion can be presented by the pose of the frame $\{B\}$ with respect to the fixed frame $\{A\}$, as shown in Fig. 1. Frame $\{B\}$ is the moving frame attached to the needle tip, and its position and orientation are representatives of the needle motion. Using this configuration, in [20] the needle is modeled as a 3D unicycle and its kinematics are expressed using coordinate free representation as

$$\dot{\boldsymbol{p}} = R \begin{bmatrix} 0 \\ 0 \\ v \end{bmatrix} \tag{1a}$$

$$\dot{R} = R \begin{bmatrix} 0 & -u & 0 \\ u & 0 & -kv \\ 0 & kv & 0 \end{bmatrix} \tag{1b}$$

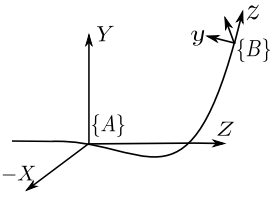

Fig. 1. The needle shown in 3D space. The frame $\{A\}$ is the fixed frame and the moving frame $\{B\}$ is attached to the needle tip.

in which the vector $\boldsymbol{p} = [x \quad y \quad z]^T$ is the needle tip position and the 3×3 rotation matrix R represents the orientation of the frame $\{B\}$ with respect to the frame $\{A\}$, respectively, and $\dot{(.)}$ denotes the time derivative. k and v are the curvature of the needle path and the insertion velocity, respectively. u denotes the needle base axial rotational velocity, which is assumed to be upper bounded by $\bar{u}$ and is the primary factor in determining the needle tip path. The insertion velocity v has minimal effect on the tip path [22] and is therefore assumed to be constant in this paper.

Remark 1. *As shown in [15], from* (1a)*, it is easy to see that the vector $\dot{\boldsymbol{p}}$ is the last column of matrix R multiplied by v. By expanding* (1b)*, the second column of R can also be presented by second time derivative of the position vector multiplied by $1/k$. Moreover, representing the ij^{th} element of the rotation matrix with r_{ij}, from the orthogonality property of the rotation matrix, the elements $r_{i1}, i = 1, 2, 3$, can be written as*

$$r_{i1} = \pm\sqrt{1 - (r_{i2}^2 + r_{i3}^2)} \tag{2}$$

The needle is inserted continuously in the Z direction without retractions until it reaches the final depth. In this case, x and y determine the needle deflection at each insertion depth. As explained in [13], the 3D needle tip position vector $\boldsymbol{p} = [x \quad y \quad z]^T$ can be found using 2D transverse ultrasound images and the image processing techniques. The 3D needle position can be projected into $X-Z$ and $Y-Z$ planes, forming 2D maps of needle deflection. Using (1) and defining the new vector $\boldsymbol{s_i} = \begin{bmatrix}\boldsymbol{p}(i) & vr_{i3} & (-kv^2)r_{i2}\end{bmatrix}$, the needle motion in the $X-Z$ plane for $i = 1$ with $\boldsymbol{s}_1 = \begin{bmatrix}x & vr_{13} & (-kv^2)r_{12}\end{bmatrix}$, and in the $Y-Z$ plane for $i = 2$ with $\boldsymbol{s}_2 = \begin{bmatrix}y & vr_{23} & (-kv^2)r_{22}\end{bmatrix}$ can be expressed in state space as

$$\dot{\boldsymbol{s}}_{\boldsymbol{i}} = A\boldsymbol{s_i} + B\phi(\boldsymbol{s_i}) \tag{3a}$$
$$y_{s_i} = C\boldsymbol{s_i} \tag{3b}$$

with

$$A = \begin{bmatrix}0 & 1 & 0\\ 0 & 0 & 1\\ 0 & 0 & 0\end{bmatrix} \tag{4a}$$
$$B = [0 \quad 0 \quad 1]^T \tag{4b}$$
$$C = [1 \quad 0 \quad 0] \tag{4c}$$
$$\phi(\boldsymbol{s_i}) = \underbrace{-(kv)^2\boldsymbol{s}_i(2)}_{\phi_L} \underbrace{\pm kv^2\sqrt{1 - \left(\frac{\boldsymbol{s}_i(2)}{v}\right)^2 + \left(\frac{\boldsymbol{s}_i(3)}{kv^2}\right)^2}\,)\,u}_{\phi_\Delta} \tag{4d}$$

Since the equations representing the planar motion have the same form for $i = 1, 2$, in the sequel, the index i is omitted for simplicity.

The new state vector $\boldsymbol{s}$ is related to the needle tip pose. Whereas the first element in $\boldsymbol{s}$, i.e., $\boldsymbol{s}(1)$ is directly measured from images, the second and third element in $\boldsymbol{s}$, which are related to rotation matrix elements, need to be estimated.

The state observer is a computer-implemented system, which runs concurrently to the real system and we have access to all its states. The observer equations are formed using the system equations (3)-(4) and an additional corrective term. If we can show the convergence of the observer, the observer states can be used as the estimated states. However, since ϕ_Δ does not satisfy the Lipschitz continuity condition, it is not possible to design a convergent observer and instead an approximate observer is used. The following section is devoted to the observer design process for the 2D case. As explained before, the 3D observation problem can be resolved to two 2D problems. Later in Section V, a controller is designed.

IV. Needle Orientation Observer

For the observable system (3)-(4), the main challenge in designing a state observer for (3) is the nonlinear term $\phi(\boldsymbol{s})$ as the function $\phi_\Delta = kv^2\sqrt{1 - ((\boldsymbol{s}(2)/v)^2 + (\boldsymbol{s}(3)/kv^2)^2)}$ is both continuous and bounded but does not satisfy the Lipschitz continuity condition when $((\boldsymbol{s}(2)/v)^2 + (\boldsymbol{s}(3)/kv^2)^2) \to 1$. To deal with this constraint, the following high-gain approximate observer is used [21]

$$\dot{\hat{\boldsymbol{s}}} = A\hat{\boldsymbol{s}} + B\phi(\hat{\boldsymbol{s}}) + \frac{1}{2}M_\theta^{-1}C^T\left(y_s - C\hat{\boldsymbol{s}}\right) \tag{5a}$$
$$\hat{y}_s = C\hat{\boldsymbol{s}} \tag{5b}$$

where A, B, C and ϕ are defined in (4) and $\hat{\boldsymbol{s}}$ is the estimated state vector. M_θ is a positive-definite matrix that satisfies the algebraic Lyapunov equation

$$-\theta M_\theta - A^T M_\theta - M_\theta A + C^T C = 0 \tag{6}$$

with $\theta > 1$. For a fixed value of θ, this equation can be rewritten as $-(I + (1/\theta)A^T)M_\theta - M_\theta(1/\theta)A + 1/\theta C^T C = 0$, which can be solved using the `lyap` function in Matlab. The last term on the right-hand side of (5) is the corrective term added to compensate for estimation errors. Defining the

estimation error as $e = \hat{\boldsymbol{s}} - \boldsymbol{s}$ and the Lyapunov function $V(e) = e^T M_\theta e$, the time derivative of $V(e)$ is obtained as

$$\dot{V}(e) = -\theta e^T M_\theta e + 2e^T M_\theta \left(\phi(u, \hat{\boldsymbol{s}}) - \phi(u, \boldsymbol{s})\right) \quad (7)$$

Since ϕ_L in (4) is a Lipschitz function with some Lipschitz constant ℓ and the non-Lipschitz term involving ϕ_Δ to be bounded by some $\sup|u\phi_\Delta| = \delta/2$, in [21] it is shown that the observation error is upper-bounded as

$$\|e\| \leq \theta^2 \left(\frac{c_2}{c_1}\right) \|e(0)\| \exp(-\mu t) + \frac{\delta \bar{M}}{c_1 \mu} \left(1 - \exp(-\mu t)\right) \quad (8)$$

In this equation, $c_1 = \sqrt{|\lambda_{min}(M_1)|}$, $c_2 = \sqrt{|\lambda_{max}(M_1)|}$, in which λ denotes the eigenvalue of the matrix and $\bar{M} = \sqrt{M_{1_{3,3}}}$, where M_1 is the solution of (6) for $\theta = 1$ and $M_{1_{3,3}}$ is (3,3) element of M_1 . Also, $\mu = \frac{1}{2}\theta - (\ell/c_1)\bar{M}$ and θ is chosen such that $\mu > 0$. In this equation, the first term exponentially approaches zero; however, the second term increases exponentially to the value $\delta\bar{M}/c_1\mu$. Therefore, there exists some $T \geq 0$ such that the observation error is upper bounded by

$$\|e(t)\| \leq \bar{\beta} \frac{\delta \bar{M}}{c_1 \mu}, \quad t \geq T \quad (9)$$

in which $\bar{\beta}$ is slightly greater than one.

V. Controller

A. Controller Structure

In this section, the introduced observer is combined and used with a controller to control the needle tip position in a plane. As stated in the previous section, assuming that the input signal u is bounded, the designed observer ensures the boundedness of the estimation error. In this section, the designed controller is nonlinear state feedback. By redefining the nonlinear term $\phi(\boldsymbol{s}) = \Omega$, (3) turns to a linear system with Ω as its input. Using this definition the control input u is found by

$$u = \frac{\Omega - \phi_L}{\phi_\Delta} \quad (10)$$

Remark 2. *The above equation can be used for finding the control signal u when $\phi_\Delta \neq 0$. However, if $\phi_\Delta \to 0$, using* (10) *is not practical as it will yield an unbounded control signal. To overcome this problem, ϕ_Δ can be replaced by ϕ'_Δ defined as*

$$\phi'_\Delta = \begin{cases} \phi_\Delta & |\phi_\Delta| > \phi_0 \\ \phi_0 & |\phi_\Delta| \leq \phi_0 \end{cases} \quad (11)$$

where ϕ_0 is a small positive number.

If Ω is bounded, (11) ensures the control signal u is bounded. In this case, the closed-loop system equation can be written as

$$\dot{\boldsymbol{s}} = A\boldsymbol{s} + B\frac{\phi_\Delta}{\hat{\phi}'_\Delta}\Omega + B(\hat{\phi}_L - \frac{\phi_\Delta \phi_L}{\hat{\phi}'_\Delta}) \quad (12)$$

where $\hat{(.)}$ represents evaluation at estimated values $\hat{\boldsymbol{s}}$. Assuming $\frac{\phi_\Delta}{\hat{\phi}'_\Delta} \to 1$, the above equation can be written as

$$\dot{\boldsymbol{s}} = A\boldsymbol{s} + B\bar{\Omega}\sigma(\Omega/\bar{\Omega}) + Ew(t) \quad (13)$$

where $\bar{\Omega} > 0$ is the upper bound of Ω. The saturation function is defined as $\sigma(t) = sign(t)min(1, |t|)$ and $w(t)$ is a disturbance term, which can include modelling and parameter uncertainty, noise and estimation error.

Remark 3. *Since the system state vector $\boldsymbol{s}$ is estimated using the observer introduced in the previous chapter, as long as the input signal to the system is bounded, the estimation error remains bounded. Remembering that the columns of a rotation matrix are unit vectors, using the assumptions $|\hat{s}_2| \leq 1 + \bar{e}$, where $\bar{e}$ is the upper bound for the observation error, the upper bound on the disturbance term can be found as*

$$|w(t)| \leq (kv)^2(1 + \bar{e}) \quad (14)$$

Here, the state feedback control law $\Omega = F\hat{\boldsymbol{s}}$ should be designed considering the saturation function and the bounded disturbance $w(t)$. Using equations (10) and (4), and substituting the state vector $\boldsymbol{s}$ with the estimated vector $\hat{\boldsymbol{s}}$, the control signal u is calculated as

$$u = \frac{F\hat{\boldsymbol{s}} + (kv)^2\hat{\boldsymbol{s}}(2)}{\hat{\phi}'_\Delta} \quad (15)$$

In (5), θ is the design parameter which determines the observer gain. From (9) it is clear that larger values of θ lead to smaller estimation error bound. Therefore, by proper selection of θ to be sufficiently large, the controller can be designed to yield a negligible tracking error. Still, it is important to remember the effect of the saturation on the state feedback should be taken into account in the controller design process.

B. Controller Design

The state feedback gain F should be designed to ensure the convergence of the response in the presence of the input saturation. The following notations are used in the sequel to re-formulate the design problem [23].

Notation. *Denoting the system trajectories starting from initial condition x_0 by $\psi(t, x_0)$, the domain of attraction of the origin (DOA) is defined as $\mathcal{J} = \{x_0 \in \boldsymbol{R}^3 : \lim_{t\to\infty} \psi(t, x_0) = 0\}$. If $w(t) = 0$, an ellipsoid $\mathcal{E}(P, \rho) = \{x \in \boldsymbol{R}^3 : x^T P x \leq \rho\}$ with P being a positive-definite matrix is contractively invariant if the time derivative of $V(x) = x^T P x$ is negative-definite for all $x \in \mathcal{E}(P, \rho)$. If $w(t) \neq 0$, an ellipsoid $\mathcal{E}(P, \rho)$ is called strictly invariant if the time derivative of $V(x) = x^T P x$ is negative-definite for all $w(t)$ with $|w(t)| < 1$ and all $x \in \partial\mathcal{E}(P, \rho)$, the boundary of $\mathcal{E}(P, \rho)$. A set is called invariant if all the trajectories starting from this set remain inside it for all times, regardless of the disturbance $w(t)$.*

Using the above notations, when $w(t) = 0$, the response convergence can be expressed as ensuring for the desired set, all the trajectories starting from this set converge to zero. The problem is then defined as designing the state feedback gain F such that a pre-defined set resides in the DOA. Moreover, in order to have some control over the convergence rate, the controller gain $F = [f_1 \quad f_2 \quad f_3]$ is designed using pole placement method. For simplicity, the feedback gain F is parameterized by a control design parameter ε to shift the

closed-loop eigenvalues by -2ε. For the matrices A and B defined in (4) the characteristic equation of the closed-loop system $A+BF$ can be found as $\lambda^3-f_3\lambda^2-f_2\lambda-f_1=0$. This equation is solved to place the eigenvalues of the closed-loop system at -2ϵ, and find the state feedback gain F_ε elements as

$$F_\epsilon = \begin{bmatrix} -8\epsilon^3 & -12\epsilon^2 & -6\epsilon \end{bmatrix} \tag{16}$$

Since in reality $w(t) \neq 0$, the state feedback control gain should be designed to ensure disturbance rejection. The problem here will be to ensure that for the designed state feedback gain, there exist two invariant sets $\mathcal{E}(P,\rho_1)$ and $\mathcal{E}(P,\rho_2)$ with $\rho_1 < \rho_2$ and ρ_1 small enough such that the system trajectories starting from $\mathcal{E}(P,\rho_2)$ enter the smaller invariant set $\mathcal{E}(P,\rho_1)$.

Lemma. *[23] Consider the system of the form* (13) *and set* $B' = B\bar{\Omega}$ *and* $F' = F/\bar{\Omega}$. *Given two ellipsoids* $\mathcal{E}(P,\rho_1)$ *and* $\mathcal{E}(P,\rho_2)$ *with* $\rho_2 > \rho_1 > 0$, *if there exist* $H_1, H_2 \in \boldsymbol{R}^{1\times n}$ *and a positive number* η *such that*

$$\begin{aligned}(A+B'M(F',H_i))^TP + P(A+B'M(F',H_i)) \\ +\frac{1}{\eta}PEE^TP + \frac{\eta}{\rho_i}P < 0 \end{aligned} \quad i=1,2 \tag{17}$$

and $\mathcal{E}(P,\rho_i) \subset \mathcal{L}(H_i)$, *where* $M(F',H) = \{H, F'\}$ *and* $\mathcal{L}(H) = \{x \in \boldsymbol{R}^n : |Hx| \leq 1\}$ *then for every* $\rho \in [\rho_1, \rho_2]$, *there exist an* H *such that* (17) *is satisfied and* $\mathcal{E}(P,\rho) \subset \mathcal{L}(H)$ *which is equivalent to* $\mathcal{E}(P,\rho)$ *being strictly invariant.*

In order to guarantee that the designed controller is convergent in presence of non-zero disturbance, it is only required to find two invariant ellipsoids $\mathcal{E}(P,\rho_1)$ and $\mathcal{E}(P,\rho_2)$ with $\rho_1 < \rho_2$ and ρ_1 small enough satisfying the conditions of the lemma. This can be expressed as the following optimization problem with LMI constraints [23]:

$$\inf_{Q>0, g_1, g_2} \quad \delta \tag{18a}$$

$$s.t.\ (a)\ \begin{bmatrix} X_{R2} & I \\ * & \rho_2 Q \end{bmatrix} \geq 0 \tag{18b}$$

$$(b)\ \begin{bmatrix} Q/\rho_1 & Q \\ * & \delta X_{R1}^{-1} \end{bmatrix} \geq 0 \tag{18c}$$

$$\begin{aligned}(c)\ & QA^T + AQ + M(F'Q, g_i)^T B'^T \\ & + B'M(F'Q, g_i) + \frac{1}{\eta}EE^T + \frac{\eta}{\rho_i}Q < 0 \end{aligned} \tag{18d}$$

$$(d)\ \begin{bmatrix} 1 & g_i \\ * & \rho_i Q \end{bmatrix} \geq 0 \tag{18e}$$

where B' and F' are defined as in (17) and $i = 1, 2$. X_{R2} and X_{R1} are estimations of the DOA and the guaranteed convergence area, respectively. For simplicity and in order to have a convex optimization, it is possible to assume $\rho_2 = 1$ and fix ρ_1 and η. Changing ρ_1 from 0 to 1 and η from 0 to ∞, the infimum δ^* can be found. This optimization, gives the positive definite matrix Q, from which the matrix P defining the two ellipsoids can be obtained by $P = Q^{-1}$.

VI. Evaluation

A. Controller Implementation and Simulations

The block diagram of the system and the proposed observer is shown in Fig. 2. In this figure, the feedback linearization is the technique used for transforming the nonlinear system into an equivalent linear system through a control input and a change of variables. In (10), Ω serves as the new input to the linearized system and is replaced with a state feedback control law in (15). According to the rotational behavior of the system, the closed-loop system acts differently from usual control systems causing the designed controller not working properly. In a usual state feedback control loop, larger errors lead to a larger control signal to put the maximum effort to compensate the error. Here, since the system states, i.e., velocity and acceleration, are related to the rotation matrix entries, their maximum and minimum are defined in a full 2π rotation, and any excessive 2π rotations cause the states to oscillate between their maximum and minimum values. To compensate this, the rotations should be limited to 2π, and large control inputs should be interpreted as maximum effort or the maximum acceleration. In the planar case, if the needle is rotated by 180°, the bevel and consequently the needle path is flipped. This can also be seen from the $\pm$ sign in (4). From here it can be seen that in order to apply the maximum effort, the bevel should be kept in one half-plane. As shown in Fig. 2, this can be done by keeping the needle base angle θ_b in one half-plane by multiplying the control input u by $sgn(\cos(\theta_b))$. Whenever the bevel passes one half-plane, u is reversed to bring it back. Also, the chattering caused by the sign function can be reduced by replacing this function with a hysteresis block.

Note that since $\phi_\Delta(\boldsymbol{s})$ is derived from the orthonormality property of the rotation matrix, it has real values. However, this might not be true for $\phi_\Delta(\hat{\boldsymbol{s}})$, as $\hat{\boldsymbol{s}}$ is the estimated vector. To deal with this, whenever $(\hat{\boldsymbol{s}}(2)/v)^2 + (\hat{\boldsymbol{s}}(3)/kv^2)^2 > 1$, we replace $\phi_\Delta(\hat{\boldsymbol{s}})$ with zero. This will not affect any of the analysis performed in the previous sections as $\phi_\Delta(\hat{\boldsymbol{s}})$ is still upper bounded, which can be used to show the boundedness of the error.

The block diagram of the system and the proposed observer is shown in Fig. 2. Using Matlab/Simulink the simulations are presented for the constant insertion velocity of 2 mm/sec, the curvature of 0.0014 mm^{-1}, and the upper bound for the rotational velocity of $\bar{u} = 3\pi$. The insertion velocity in clinical needle insertions vary between 5 and 50 mm/sec [24]. However, compensating the deflection error using axial rotations can only be effective if the commanded rotations are performed accurately at each insertion depth, which requires the rotations to be fast enough with respect to the insertion velocity. Due to the limit on the needle axial rotational velocity, we selected the insertion velocity slightly lower than the clinically used values both in simulations and experiments. The needle curvature is also chosen from previous works on the needle deflection modelling, which have experimentally reported a mean radius of curvature of 650 mm for 18G brachytherapy needles [25], [26]. Using these values the observer parameter θ is selected as 15 for which using (9), the upper bound of error norm is

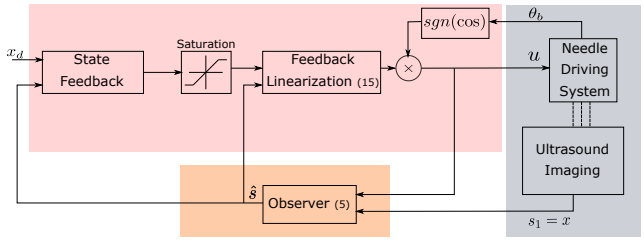

Fig. 2. The block diagram of the observer/controller loop.

obtained as 0.03.

To find the state feedback gain F and the guaranteed DOA and the disturbance rejection area, ρ_1 is fixed to 0.03 and F is found by varying ε in (16) and solving the optimization (18) for $X_{R1} = I_{3\times3}$, $X_{R2} = diag(0.1, 1, 50)$ and different values of η such that the LMI constraints are feasible. The results are shown in Fig. 3(a). The value of ε which gives the minimum value of δ^* is selected for finding the controller gain. Fig. 3(b) and 3(d) also represent the guaranteed DOA and the disturbance rejection area. Note that these results show the conservative guaranteed convergence region. Before proceeding to experiments, in order to see the performance of the observer/controller structure, simulations are presented for different values ϵ to steer the needle along the x-axis with the desired value of $x_d = 3$ mm. The value of the curvature used in the observer equations is considered with 10% uncertainty. In real applications, there might be a difference between the initial values of the needle and the observer. Since the needle is inserted without any initial bending, the initial conditions are selected as $x_0 = -0.5$ mm and $\theta_{b0} = 10^\circ$ for the needle, and zero for the observer. The results in Fig. 3(c) shows that for different values of ϵ the needle position moves towards the desired value and increasing the gain leads to a faster response. It should be noted that in simulations the rotations are ideal and the signals are noise-free.

B. Experiments

In this section, the proposed observer and controller are implemented in real-time for estimating the needle tip states and controlling the out-of-plane deflection of the needle tip. The experimental setup used for conducting the experiments is a 2-DOF prismatic-revolute robotic system shown in Fig. 4. A DC motor actuates the translational carriage, and the rotational stage is actuated by a second DC motor to perform needle base axial rotations. A proportional-integral-derivative (PID) controller is used to control the position of this second motor. Considering the physical system limitations, the control input u is bounded to $\pi/2$. The needles used in the experiments are standard 18-gauge brachytherapy needles (Eckert & Ziegler BEBIG Inc., Oxford, CT, USA) made of stainless steel, with an outer diameter of 1.27 mm, an inner diameter of 1 mm, and a bevel angle of approximately 20°. During the insertion, the ultrasound probe tracks the needle tip and acquires 2D transverse images of the needle. The 3D needle tip position is then obtained from partial observations in 2D ultrasound transverse images using the random sample

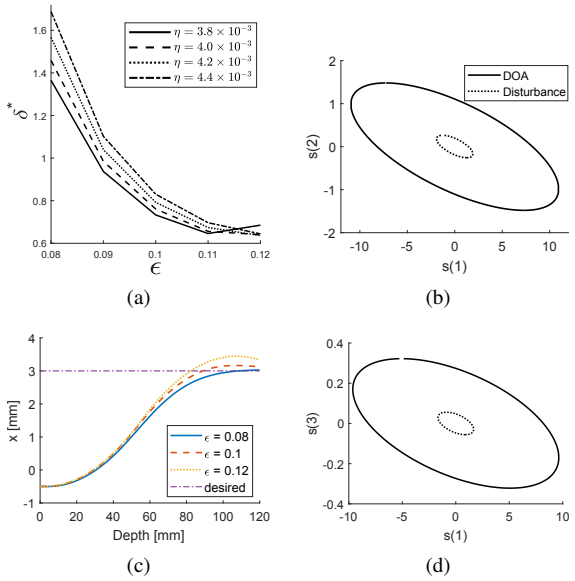

Fig. 3. State feedback design and its effect on DOA. (a): The effect of different values of ε on δ^* for different values of η. (b),(d): The 2D projection of the DOA and the guaranteed disturbance rejection area for $\varepsilon = 0.11$. (c): Simulation results for desired value $x_d = 3$ mm and different values of ϵ

consensus (RANSAC) technique [13]. Moreover, since the obtained position data are noisy, the position data is filtered before applying to the observer. The needle path curvature k is 0.002 mm^{-1} which is obtained by inserting the needle into tissue without any axial rotations and by fitting a circle to the tip deflection data. The needles are inserted with a constant velocity of 2 mm/sec and to the maximum insertion depth of 120 mm. Two different goals are considered, and for each goal, eight trials are performed. The first goal involves keeping the needle deflection equal to zero or keeping the needle in one plane. The second goal is to steer the needle to the desired deflection of 3 mm, which can be interpreted as compensating the initial insertion error. Both cases are implemented using two different tissues. The first tissue is plastisol phantom tissue, which is the combination of 80% liquid plastic and 20% plastic softner (M-F Manufacturing Co., Fort Worth, TX, USA). The Young's modulus of elasticity of the tissue is 40 kPa. Both cases are also implemented on the biological tissue (beef) embedded into 15% gelatin mixture to simulate a 2-layer non-homogeneous tissue. Fig. 5(a)-5(l) present the experimental results. These figures show the planar deflection error for eight trials, the real needle position, the estimated position, and the needle base angel for one trial as an example. Though other states estimated by the observer are used in calculating the control signal, the responses are not shown here as there are no ground truth measurements available for comparison. The summary of the results is shown in table I. As the results show, the mean final deflection error and the maximum final error are 0.73 mm and 1.24 mm, respectively. In this application, the acceptable error range is selected as 2 mm, which is the size of the smallest lesion that

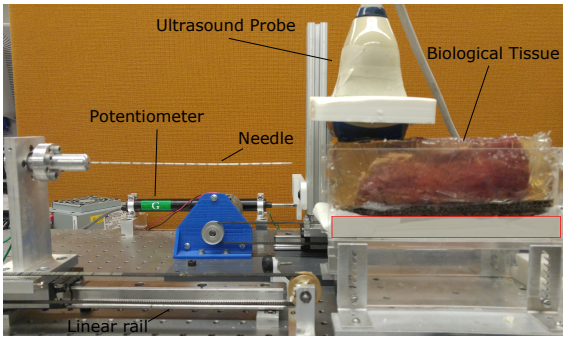

Fig. 4. Experimental setup used for implementing the needle insertion experiments. The ultrasound probe (SonixTouch, Ultrasonix, BC, Canada) tracks the needle as inserted into the tissue.

TABLE I. SUMMARY OF THE EXPERIMENTAL RESULTS

Tissue	x_d [mm]	Mean Absolute Error [mm]	Standard Deviation σ	Root Mean Square Error	Mean Final Error [mm]	Max Final Error [mm]
Phantom Tissue	0	0.27	0.44	0.5	0.49	0.71
	3	1.58	1.05	1.8	0.36	0.99
Biological Tissue	0	0.51	0.43	0.62	0.73	1.24
	3	1.6	1.01	1.9	0.53	1.22

can be detected by ultrasound images [27]. Using the multi-layer biological tissue, due to the higher parametric uncertainty cause by tissue non-homogeneity, the errors are slightly higher than errors obtained from the phantom tissues. However, the errors are still in the acceptable range.

The average seed placement error in manual insertions performed by expert surgeons is the order of 5-6.3 mm [28], [29]. Comparing these values with the results obtained in this work, shows the ability of the proposed method in improving the needle tip positioning.

C. Comparison

In this section, we provide a comparison of the proposed method with other methods in the literature. The linear observer, which is mostly used in the other works, is found by linearizing the system equations and is combined with different planning and control methods as explained in section I. The linear observer is locally convergent, and its application is limited to stabilizing the motion in one plane. Our observer, on the other hand, does not impose such a limitation on the needle workspace at the expense of just bounding the observation error and imposing bounds on the control input. However, this is not very limiting as due to the actuator saturation, bounding the control input is acceptable. Moreover, the bounds on the estimation error depend on the observer gain and can be made small by proper selection of the design parameter θ. In addition, comparing the results from the observer/controller structure with other methods proposed in the literature indicates that the results are in the same range obtained in other studies, reporting a maximum final error of 1.3 mm in [4], where the orientation information is obtained using a 5DOF sensor.

VII. CONCLUDING REMARKS

In this work, 3D unicycle needle equations are used, and it is shown that without any change in the variables, the equations represent partially linear sets of equations, which incorporate both position and orientation data. Using this format, a high gain observer is designed to deal with the non-Lipschitz property of the equations and estimate the needle tip pose. Using LMI optimizations, the 2D controller is designed for compensating the out-of-plane deflection. The performance of the proposed observer/controller combination is verified using simulations and experiments for different cases. The controller proposed in this paper only considers the out-of-plane motion of the needle. Since using observers in a controller loop requires stability proof of the whole loop, further studies are required to combine this structure with 3D needle controllers.

REFERENCES

[1] K. R. Henken, J. Dankelman, J. J. van den Dobbelsteen, L. K. Cheng, and M. S. van der Heiden, "Error analysis of fbg-based shape sensors for medical needle tracking," *IEEE/ASME Transactions on Mechatronics*, vol. 19, no. 5, pp. 1523–1531, 2014.

[2] Y. Zhao, C. Cachard, and H. Liebgott, "Automatic needle detection and tracking in 3D ultrasound using an ROI-based ransac and kalman method," *Ultrasonic imaging*, vol. 35, no. 4, pp. 283–306, 2013.

[3] N. Shahriari, W. Heerink, T. van Katwijk, E. Hekman, M. Oudkerk, and S. Misra, "Computed tomography (CT)-compatible remote center of motion needle steering robot: Fusing ct images and electromagnetic sensor data," *Medical Engineering & Physics*, vol. 45, pp. 71–77, 2017.

[4] D. C. Rucker, J. Das, H. B. Gilbert, P. J. Swaney, M. I. Miga, N. Sarkar, and R. J. Webster, "Sliding mode control of steerable needles," *IEEE Transactions on Robotics*, vol. 29, no. 5, pp. 1289–1299, 2013.

[5] B. Jiang, W. Gao, D. Kacher, E. Nevo, B. Fetics, T. C. Lee, and J. Jayender, "Kalman filter-based em-optical sensor fusion for needle deflection estimation," *International journal of computer assisted radiology and surgery*, vol. 13, no. 4, pp. 573–583, 2018.

[6] N. Abolhassani, R. V. Patel, and F. Ayazi, "Minimization of needle deflection in robot-assisted percutaneous therapy," *The international journal of medical Robotics and computer assisted surgery*, vol. 3, no. 2, pp. 140–148, 2007.

[7] G. J. Vrooijink, M. Abayazid, S. Patil, R. Alterovitz, and S. Misra, "Needle path planning and steering in a three-dimensional non-static environment using two-dimensional ultrasound images," *The International journal of robotics research*, vol. 33, no. 10, pp. 1361–1374, 2014.

[8] M. Abayazid, G. J. Vrooijink, S. Patil, R. Alterovitz, and S. Misra, "Experimental evaluation of ultrasound-guided 3D needle steering in biological tissue," *International journal of computer assisted radiology and surgery*, vol. 9, no. 6, pp. 931–939, 2014.

[9] M. Khadem, C. Rossa, N. Usmani, R. S. Sloboda, and M. Tavakoli, "A two-body rigid/flexible model of needle steering dynamics in soft tissue," *IEEE/ASME Transactions on Mechatronics*, vol. 21, no. 5, pp. 2352–2364, 2016.

[10] B. Fallahi, C. Rossa, R. S. Sloboda, N. Usmani, and M. Tavakoli, "Sliding-based switching control for image-guided needle steering in soft tissue," *IEEE Robotics and Automation Letters*, vol. 1, no. 2, pp. 860–867, 2016.

[11] V. Kallem and N. J. Cowan, "Image guidance of flexible tip-steerable needles," *IEEE Transactions on Robotics*, vol. 25, no. 1, pp. 191–196, 2009.

[12] M. Motaharifar, H. A. Talebi, F. Abdollahi, and A. Afshar, "Nonlinear adaptive output-feedback controller design for guidance of flexible needles," *IEEE/ASME Transactions on Mechatronics*, vol. 20, no. 4, pp. 1912–1919, 2015.

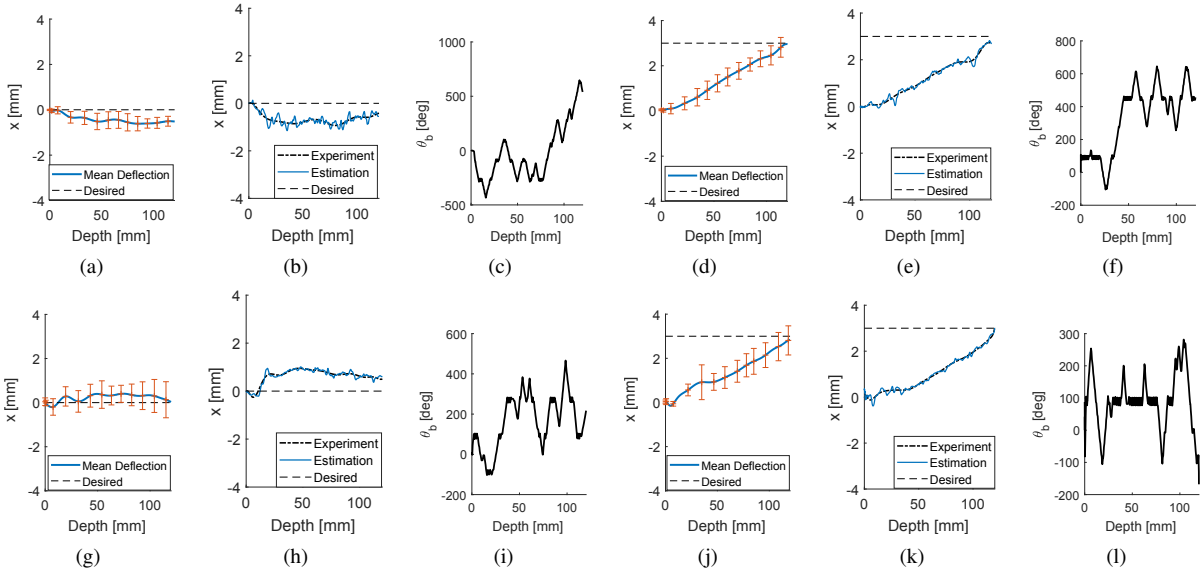

Fig. 5. Experimental results for insertion velocity of 2 mm and insertion depth of 120 mm in different tissues and different cases. (a), (b), (c): Inserting the needle into phantom tissue with $x_d = 0$ mm, representing the average deflection for different trials, one sample trial and the needle base angle, respectively. (d), (e), (f): Inserting the needle into phantom tissue with $x_d = 3$ mm, representing the average deflection for trials, one sample trial and the needle base angle, respectively. (g), (h), (i):Inserting the needle into biological tissue with $x_d = 0$ mm, representing the average deflection for different trials, one sample trial and the needle base angle, respectively. (j), (k), (l): Inserting the needle into biological tissue with $x_d = 3$ mm, representing the average deflection for different trials, one sample trial and the needle base angle, respectively. The error bars denote the standard deviation of the experimental data.

[13] M. Waine, C. Rossa, R. Sloboda, N. Usmani, and M. Tavakoli, "3D shape visualization of curved needles in tissue from 2D ultrasound images using ransac," in *IEEE International Conference on Robotics and Automation (ICRA), 2015*. IEEE, 2015, pp. 4723–4728.

[14] K. B. Reed, V. Kallem, R. Alterovitz, K. Goldbergxz, A. M. Okamura, and N. J. Cowan, "Integrated planning and image-guided control for planar needle steering," in *2nd IEEE RAS & EMBS International Conference on Biomedical Robotics and Biomechatronics, 2008. BioRob 2008.* IEEE, 2008, pp. 819–824.

[15] V. Kallem, D. E. Chang, and N. J. Cowan, "Observer design for needle steering using task-induced symmetry and reduction," *IFAC Proceedings Volumes*, vol. 44, no. 1, pp. 8028–8033, 2011.

[16] J. P. Swensen, M. Lin, A. M. Okamura, and N. J. Cowan, "Torsional dynamics of steerable needles: modeling and fluoroscopic guidance," *IEEE Transactions on Biomedical Engineering*, vol. 61, no. 11, pp. 2707–2717, 2014.

[17] G. Lapouge, J. Troccaz, and P. Poignet, "Multi-rate unscented kalman filtering for pose and curvature estimation in 3D ultrasound-guided needle steering," *Control Engineering Practice*, vol. 80, pp. 116–124, 2018.

[18] B. Fallahi, C. Rossa, R. Sloboda, N. Usmani, and M. Tavakoli, "Partial estimation of needle tip orientation in generalized coordinates in ultrasound image-guided needle insertion," in *IEEE International Conference on Advanced Intelligent Mechatronics (AIM), 2016*. IEEE, 2016, pp. 1604–1609.

[19] M. Motaharifar, H. A. Talebi, A. Afshar, and F. Abdollahi, "Adaptive observer-based controller design for a class of nonlinear systems with application to image guided control of steerable needles," in *American Control Conference (ACC), 2012*. IEEE, 2012, pp. 4849–4854.

[20] R. J. Webster, J. S. Kim, N. J. Cowan, G. S. Chirikjian, and A. M. Okamura, "Nonholonomic modeling of needle steering," *The International Journal of Robotics Research*, vol. 25, no. 5-6, pp. 509–525, 2006.

[21] A. Vargas and J. A. Moreno, "Approximate high-gain observers for non-lipschitz observability forms," *International Journal of Control*, vol. 78, no. 4, pp. 247–253, 2005.

[22] R. J. Webster, J. Memisevic, and A. M. Okamura, "Design considerations for robotic needle steering," in *Proceedings of the IEEE International Conference on Robotics and Automation, ICRA 2005.* IEEE, 2005, pp. 3588–3594.

[23] T. Hu, Z. Lin, and B. M. Chen, "An analysis and design method for linear systems subject to actuator saturation and disturbance," *Automatica*, vol. 38, no. 2, pp. 351–359, 2002.

[24] T. Podder, D. Clark, D. Fuller, J. Sherman, W. S. Ng, L. Liao, D. Rubens, J. Strang, E. Messing, Y. Zhang *et al.*, "Effects of velocity modulation during surgical needle insertion," in *2005 IEEE Engineering in Medicine and Biology 27th Annual Conference*. IEEE, 2006, pp. 5766–5770.

[25] M. Khadem, C. Rossa, N. Usmani, R. S. Sloboda, and M. Tavakoli, "Robotic-assisted needle steering around anatomical obstacles using notched steerable needles," *IEEE journal of biomedical and health informatics*, vol. 22, no. 6, pp. 1917–1928, 2018.

[26] M. Khadem, B. Fallahi, C. Rossa, R. S. Sloboda, N. Usmani, and M. Tavakoli, "A mechanics-based model for simulation and control of flexible needle insertion in soft tissue," in *IEEE International Conference on Robotics and Automation (ICRA), 2015*. IEEE, 2015, pp. 2264–2269.

[27] P. Moreira and S. Misra, "Biomechanics-based curvature estimation for ultrasound-guided flexible needle steering in biological tissues," *Annals of biomedical engineering*, vol. 43, no. 8, pp. 1716–1726, 2015.

[28] R. Taschereau, J. Pouliot, J. Roy, and D. Tremblay, "Seed misplacement and stabilizing needles in transperineal permanent prostate implants," *Radiotherapy and Oncology*, vol. 55, no. 1, pp. 59–63, 2000.

[29] P. Blumenfeld, N. Hata, S. DiMaio, K. Zou, S. Haker, G. Fichtinger, and C. M. Tempany, "Transperineal prostate biopsy under magnetic resonance image guidance: a needle placement accuracy study," *Journal of Magnetic Resonance Imaging: An Official Journal of the International Society for Magnetic Resonance in Medicine*, vol. 26, no. 3, pp. 688–694, 2007.